

Exact quantum critical states with a superconducting quantum processor

Wenhui Huang,^{1,2,3,*} Xin-Chi Zhou,^{4,5,*} Libo Zhang,^{1,2,3,*} Jiawei Zhang,^{1,2,3,*} Yuxuan Zhou,^{2,*} Zechen Guo,^{1,2,3} Bing-Chen Yao,⁴ Peisheng Huang,^{6,2} Qixian Li,^{1,2,3} Yongqi Liang,^{1,2,3} Yiting Liu,^{1,2,3} Jiawei Qiu,^{1,2,3} Daxiong Sun,^{1,2,3} Xuandong Sun,^{1,2,3} Zilin Wang,^{6,2} Changrong Xie,^{1,2,3} Yuzhe Xiong,^{1,2,3} Xiaohan Yang,^{1,2,3} Jiajian Zhang,^{1,2,3} Zihao Zhang,^{1,2,3} Ji Chu,² Weijie Guo,² Ji Jiang,^{1,2,3} Xiayu Linpeng,² Wenhui Ren,² Yuefeng Yuan,² Jingjing Niu,^{2,7} Ziyu Tao,^{2,†} Song Liu,^{1,2,3,7,‡} Youpeng Zhong,^{2,7,§} Xiong-Jun Liu,^{4,5,2,¶} and Dapeng Yu^{2,7,**}

¹Shenzhen Institute for Quantum Science and Engineering, Southern University of Science and Technology, Shenzhen 518055, China

²International Quantum Academy, Shenzhen 518048, China

³Guangdong Provincial Key Laboratory of Quantum Science and Engineering, Southern University of Science and Technology, Shenzhen 518055, China

⁴International Center for Quantum Materials and School of Physics, Peking University, Beijing 100871, China

⁵Hefei National Laboratory, Hefei 230088, China

⁶School of Physics, Ningxia University, Yinchuan 750021, PR China

⁷Shenzhen Branch, Hefei National Laboratory, Shenzhen 518048, China

(Dated: February 27, 2025)

Anderson localization physics features three fundamental types of eigenstates: extended, localized, and critical. Confirming the presence of critical states necessitates either advancing the analysis to the thermodynamic limit or identifying a universal mechanism which can determine rigorously these states. Here we report the unambiguous experimental realization of critical states, governed by a rigorous mechanism for exact quantum critical states, and further observe a generalized mechanism that quasiperiodic zeros in hopping couplings protect the critical states. Leveraging a superconducting quantum processor with up to 56 qubits, we implement a programmable mosaic model with tunable couplings and on-site potentials. By measuring time-evolved observables, we identify both delocalized dynamics and incommensurately distributed zeros in the couplings, which are the defining features of the critical states. We map the localized-to-critical phase transition and demonstrate that critical states persist until quasiperiodic zeros are removed by strong long-range couplings, confirming the generalized mechanism. Finally, we resolve the energy-dependent transition between localized and critical states, revealing the presence of anomalous mobility edges.

Introduction. In an ideal crystal, electrons experience a spatially periodic potential and are characterized by Bloch states that possess lattice translational symmetry, extending uniformly throughout the material. Introducing disorder breaks the translational symmetry, impeding the extension of the wave functions, thereby localizing the electronic states; this is known as Anderson localization^{1–5}. The states at the extended-localized transition, however, are neither fully extended nor localized, but are in a critical phase. The quantum critical phase is one of the fundamental phases in Anderson localization physics^{6–11}, surpassing the complexity of the extended and localized phases^{12–17}, and has attracted considerable interest¹⁸. This phase manifests as delocalized matter waves in both position and momentum spaces with local scale invariance as shown in Fig. 1a–c, reflecting the interplay between self-duality and multifractal structures^{19–23}. The inclusion of interactions further enriches the physics of the critical phase, with multifractality of the wave function influencing both ground

state properties associated with exotic symmetry breaking^{18,24–28} and the emergence of non-ergodic many-body critical phases²⁹ at infinite temperature that defies the eigenstate thermalization hypothesis^{30–33}.

However, confirming the existence of critical states is significantly challenging. The localized and extended state wave-functions severely fluctuate when the corresponding localization length or correlation length is comparable to the system size. Such fluctuations make localized and extended states resemble critical states. Due to this subtle nature, a precise theoretical framework to characterize such phases has been elusive for decades. Recent breakthroughs, particularly Avila’s global theory, have provided rigorous insights into the characterization of critical states in quasiperiodic systems^{11,34}. This theory establishes a universal mechanism that critical states can emerge when the couplings in one-dimensional (1D) systems are quasiperiodic and feature incommensurately distributed zeros (IDZs) in the thermodynamic limit¹¹ as illustrated in Fig. 1b, c. Experimentally, identifying critical states presents comparable difficulties. Pioneering experimental efforts have been devoted to probing critical phase^{35–39} in quasiperiodic systems^{40–48}. However, the limited system sizes in experiments introduce severe finite-size effects, causing localized and extended states to exhibit behaviors akin to critical states³⁹. This makes the rigorous experimental confirmation of critical

* These authors contributed equally to this work.

† taoziyu@iqasz.cn

‡ lius3@sustech.edu.cn

§ zhongyopeng@iqasz.cn

¶ xiongjunliu@pku.edu.cn

** yudapeng@iqasz.cn

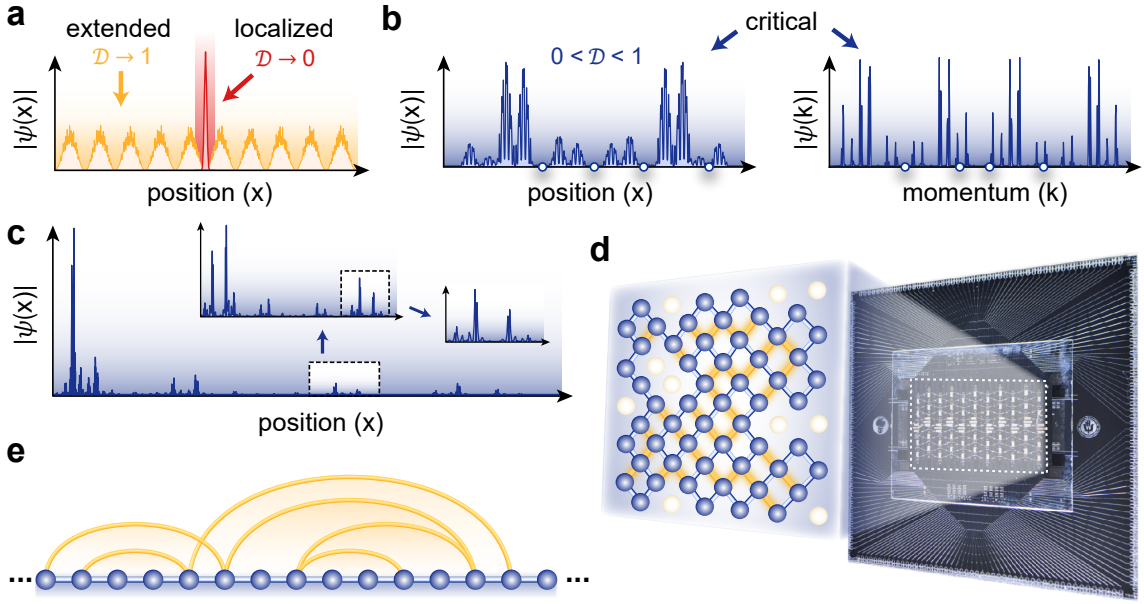


FIG. 1. **Schematic for the mechanism of quantum critical states.** **a-b** Density profile of the eigenstates in extended, localized (**a**) and critical phases (**b**), which are delocalized in both position and momentum space. Blue circles denote the incommensurately distributed zeros (IDZs), which are key ingredients for the critical states. **c** Visualization of the self-similar structure characteristic of critical states. **d** The quantum processor comprising a 2D array of 66 superconducting qubits. Blue spheres represent lattice sites, and blue (orange) bonds mark the nearest-neighbour (long-range) couplings controlled by tunable couplers in the experiment. **e** Illustration of one-dimensional chain model incorporating long-range couplings. The 2D geometry of superconducting chip facilitates long-range couplings. By activating orange bonds in 2D array and relabeling the system as a 1D chain, nearest-neighbour couplings effectively realize long-range interactions within the redefined 1D configuration.

states a challenging task. Despite these obstacles, the elusive observation of transition energies threshold linked to critical states, referred to as anomalous mobility edges (MEs), remains an area ripe for investigation.

In this work, we report the precise characterization of quantum critical states with smoking-gun evidence and further explore their universal behaviors in a mosaic model¹¹ using a superconducting quantum processor^{49–71}, which reveals universal rigorous mechanism of such critical states as well as the associated mobility edges. With the site-resolved controllability of the coupling strength on each qubit^{70–72}, we firstly observe the delocalized (localized) dynamics and confirm the presence of IDZs in coupling, providing rigorous evidence of the critical (localized) phase for the quasiperiodic mosaic models. We perform the quantum simulation on a superconducting quantum processor comprising a two-dimensional (2D) array of tunably coupled qubits, which enables us to emulate the processes with long-range coupling beyond previous quantum simulations in the one-dimensional chain as illustrated in Fig. 1d. Switching on long-range couplings, we demonstrate how the IDZs can protect critical states, as long as they are not completely removed. We further examine the elimination of IDZs in the ergodic dynamics and observe the breakdown of localized-critical phase transition when the IDZs disappear, confirming the IDZs to be a central ingredient of

the universal mechanism for stabilizing the non-ergodic critical states. Finally, we observe the anomalous mobility edges separating critical from localized states in the spectra by precisely controlling the coupling coefficients and on-site potentials to the exactly solvable point, which match the results predicted in the thermodynamic limit. This work sets a standard for the unambiguous experimental detection and characterization of quantum critical states, offering a systematic methodology for their observation, and also presents a tunable quantum platform to further explore the novel physics of the critical states.

Programmable long-range mosaic model. The model studied in the experiment is effectively described by the Hamiltonian of a 1D chain with N qubits

$$H = \sum_{j=1}^{N-1} J_j (\sigma_j^+ \sigma_{j+1}^- + \sigma_j^- \sigma_{j+1}^+) + \sum_{j=1}^N V_j \sigma_j^+ \sigma_j^- + \sum_{m,n} J_{m,n}^L (\sigma_m^+ \sigma_n^- + \sigma_m^- \sigma_n^+), \quad (1)$$

where σ_j^+ (σ_j^-) represents the raising (lowering) operator for qubits. The first term describes the nearest-neighbour (NN) coupling, with a mosaic quasiperiodic coupling which exhibits IDZs, defined as

$$J_j = \begin{cases} \lambda & j = 1 \pmod{2}, \\ 2J \cos(2\pi\alpha j + \theta) & j = 0 \pmod{2}. \end{cases} \quad (2)$$

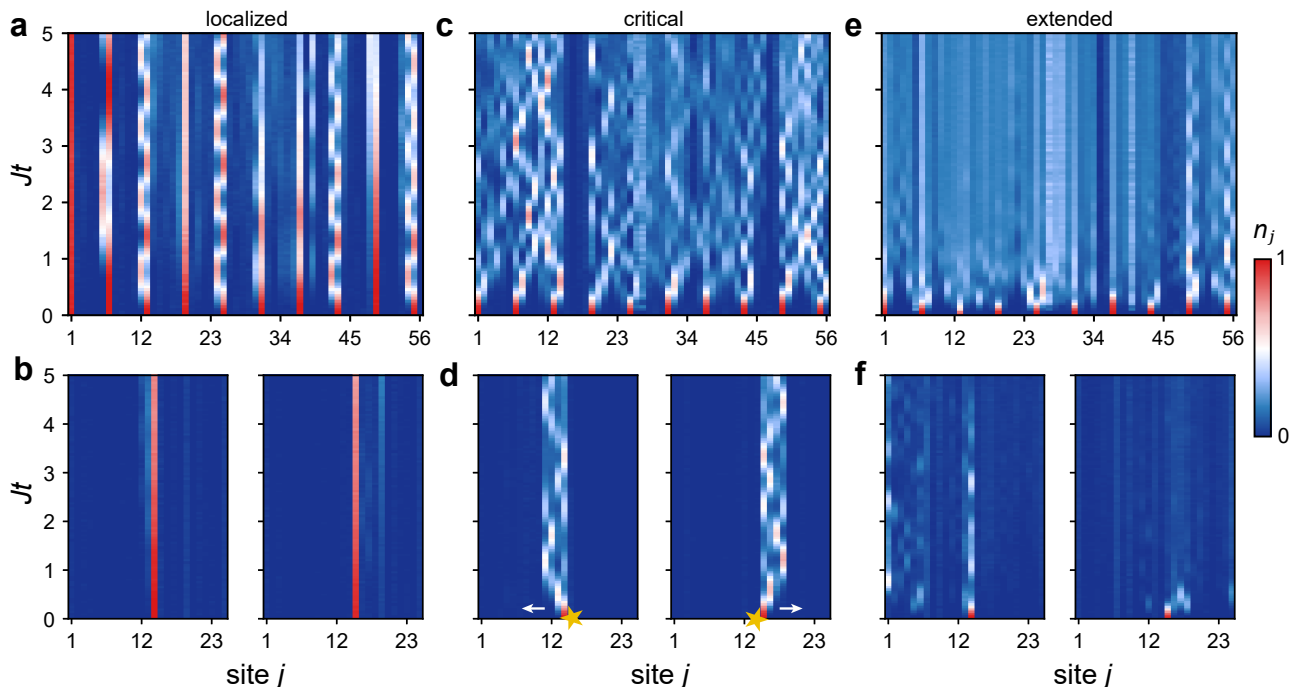


FIG. 2. **Characteristic dynamics of localized, critical and extended phases.** **a-b** Dynamics in the localized phase with $\lambda/J = 0.25$. **c-d** Dynamics in the critical phase with $\lambda/J = 2.5$. **e-f** Dynamics in the extended phase with the long-range coupling $J_{m,n}^L = \lambda$ and $\lambda/J = 2.5$. In **a,c,e**, the top panels show illustrations for the density profiles of each phase, and bottom panels show the measured dynamics of on-site population $n_j(t)$, where the system is initialized in $|\psi(t=0)\rangle = (\prod \sigma_{6k-5}^+) |0^{\otimes N}\rangle$, with k indexing every sixth site starting from site 1. **b,d,f** show the measured dynamics of $n_j(t)$ with the initial state prepared at the left and right to the zeros in coupling coefficients marked by the stars, highlighting the distinct behaviors of different phases. The parameters of systems are $\lambda/(2\pi) = 1$ MHz (localized phase), $\lambda/(2\pi) = 10$ MHz (critical phase), $\lambda/(2\pi) = J_{m,n}^L/(2\pi) = 10$ MHz (extended phase), $J/(2\pi) = 4$ MHz, $V_0 = 0$ and $\theta = \pi/5$.

Here λ and J denote NN coupling strengths, the irrational frequency $\alpha = (\sqrt{5} - 1)/2$, and θ is the phase offset. The second term is a mosaic on-site potential

$$V_j = \begin{cases} 2V_0 \cos[2\pi\alpha(j-1) + \theta] & j = 1 \pmod{2}, \\ 2V_0 \cos(2\pi\alpha j + \theta) & j = 0 \pmod{2}, \end{cases} \quad (3)$$

with amplitude V_0 . The long-range coupling $J_{m,n}^L$ is introduced via tunable couplers $C_{m,n}$ connecting qubits with indices m and n on a 2D lattice configuration, as shown in Fig. 1d, e. This long-range coupling enables the exploration of mechanisms underlying the rigorous critical states and serves as a switch to include extended states in the system. In the limit of short-range coupling $J_{m,n}^L = 0$ and uniform potential $V_0 = 0$, the system is exactly solvable and exhibits a phase transition between localized and critical phases at $\lambda = J$. The localized phase is obtained for $\lambda < J$, with localization length $\xi = 2/\log|J/\lambda|$, and the critical phase for $\lambda > J$ (see Supplemental Information). The critical states arise from the generic mechanism of combining the delocalized nature of the states and the IDZs in the coupling coefficients J_j . Turning on the long-range coupling may remove the IDZs and drive the critical phase into extended phase. On the other hand, introducing a quasiperiodic on-site potential leads to energy-dependent transitions between

localized and critical states, where the transition energies E_c define the mobility edges. Interestingly, along the high-symmetric line $V_0 = J$, the system becomes exactly solvable again, allowing for an analytical determination of the localization properties of all eigenstates.

In the experiment, all coupling coefficients and on-site potentials are independently tunable, which we utilize to unravel the mechanism underlying the critical states. We first demonstrate the fundamental organizing principle for the critical states by toggling the long-range coupling in the uniform potential limit $V_0 = 0$, highlighting the key role played by the IDZs for realizing the critical states. Following this, we map out the complete phase diagram for the localized-to-critical phase transition. Finally, we probe the MEs by adjusting the on-site potential, further showcasing the precise tunability of the system.

Universal mechanism for critical states. We first identify the key mechanism relating the critical states to the presence of IDZs by studying the characteristic dynamics of different types of states. The time evolution of density population $n_j(t) = |\langle \psi(t) | 1_j \rangle|^2$ with $|1_j\rangle = \sigma_j^+ |0^{\otimes N}\rangle$, reveals the unique localization properties of different states as shown in Fig. 2. Here $|\psi(t)\rangle = \exp(-iHt)|\psi(0)\rangle$, and $|\psi(0)\rangle$ is the initial state. Without the on-site modulation and long-range couplings, we

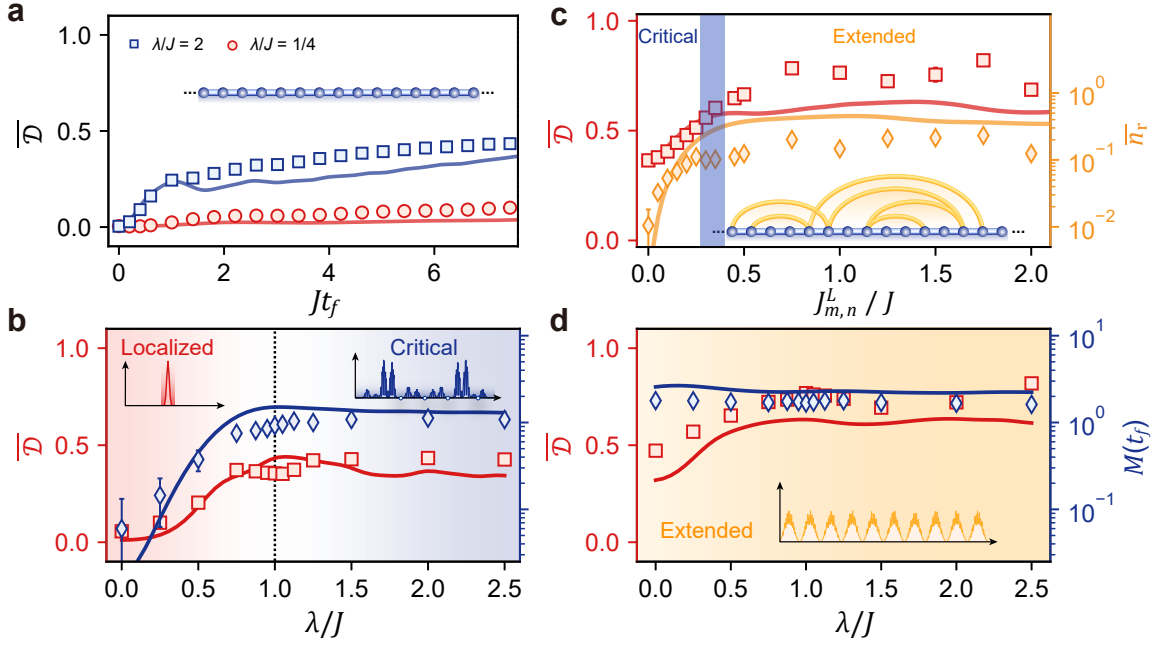


FIG. 3. **Localized-critical phase transition and its breakdown.** **a** Measured time-averaged observable $\overline{\mathcal{D}}$ within the time range from 0 to t_f for long-ranged coupling $J_{m,n}^L = 0$, where $\lambda/J = 1/4$ ($\lambda/J = 2$) are chosen from a deeply localized (critical) phase. **b-d** Characterization of the localized-critical phase transition for $J_{m,n}^L = 0$ (**b**) and its breakdown in the presence of long-ranged coupling (**c-d**), where (**c**) shows $\overline{\mathcal{D}}$ and time-averaged $\bar{n}_r = \sum_{j>j_0} n_j$ for different $J_{m,n}^L/J$ with $\lambda = 10$ MHz, and (**d**) gives $\overline{\mathcal{D}}$ and $M(t_f)$ for different λ/J with $J_{m,n}^L = 2.5J$. The system is initialized in $|\psi(t=0)\rangle = |1\rangle_{14}$, $J/(2\pi) = 4$ MHz, and the size of system is $N = 24$. The markers represent experimental data, and the solid lines correspond to simulations.

observe only the localized and critical dynamics. In particular, for the localized phase with $J > \lambda$, the density profile remains confined as shown in Fig. 2a, b. The localization can be understood as follows. Diagonalizing the dominant $J_j = 2J \cos(2\pi\alpha j)$ term in Hamiltonian Eq. (1) yields disconnected dimers with quasiperiodically distributed energies, which act as an incommensurate on-site potential. The smaller uniform coupling $J_j = \lambda$ connects these dimers, and the system resembles double Aubry-André chain⁴¹ in localization phase. In comparison, for critical phase with $J < \lambda$ in Fig. 2c, d, the quantum states propagate while preserving their local configurations, indicating a critical behavior. Finally, when the long-range coupling is turned on and $J_{m,n}^L = \lambda$, the density profile rapidly expands over the entire system (see Fig. 2e, f), erasing the initial configuration and manifesting an extended phase.

The emergence of the critical states is observed uniquely connecting to IDZs, as located in bonds at sites $j = 14$ and $j = 47$ in our sample, through which the tunneling takes longest time (Fig. 2c,d). The nearly vanishing tunneling leads to the unique uni-side quantum dynamics. The lower panel of Fig. 2 depicts the single-spin evolution with initial states $|\psi(t=0)\rangle = |1\rangle_{14}$ and $|1\rangle_{15}$, respectively. For critical phase, we observe that the wave-packet propagates in one side of the bond connecting sites $j = 14$ and 15 , with negligible probability in another side (see Fig. 2d). This uni-side propagation

quantum dynamics provides a characteristic signature to identify and benchmark IDZs within the system. In contrast, for the long-range coupling $J_{m,n}^L = \lambda$, the uni-side quantum dynamics breaks down, with the propagation across the bond at $j = 14$ being clearly observed (Fig. 2f). Thus the IDZs disappear and the system turns to extended phase (Fig. 2e). The distinct quantum dynamics associated with the IDZs enables a comprehensive exploration of the entire phase diagram based on the present programmable 2D sample by tuning the long-range couplings.

Localized-critical-extended phase transitions.

We then investigate the phase transition between localized and critical states by mapping out the full phase diagram for the mosaic model with $V_0 = 0$. To characterize the transition, we employ the time-averaged observable $\overline{\mathcal{D}} = (1/t_f) \int_0^{t_f} [\mathcal{D}(\tau) - \mathcal{D}(0)] d\tau$ and the integrated width $M(t_f)$ within the time range from 0 to t_f . Here the observable \mathcal{D} for the state $|\psi_m\rangle = \sum_{j=1}^N u_{m,j} \sigma_j^+ |0^{\otimes N}\rangle$ is defined as $\mathcal{D} = -\log \sum_j |u_{m,j}|^4 / \log N$ in analog with the form of fractal dimension which quantifies the effective spatial dimension of the state [see Supplemental Information]. Given that \mathcal{D} is always between 0 and 1 for the finite system size, we also introduce the integrated width $M(t_f) = (1/t_f) \int_0^{t_f} [W(\tau) - W(0)] d\tau$, where $W(\tau) = \sum_j \sqrt{|j - j_0|} \langle n_j(\tau) \rangle$, which characterizes the expansion of the spin transport initially located at j_0

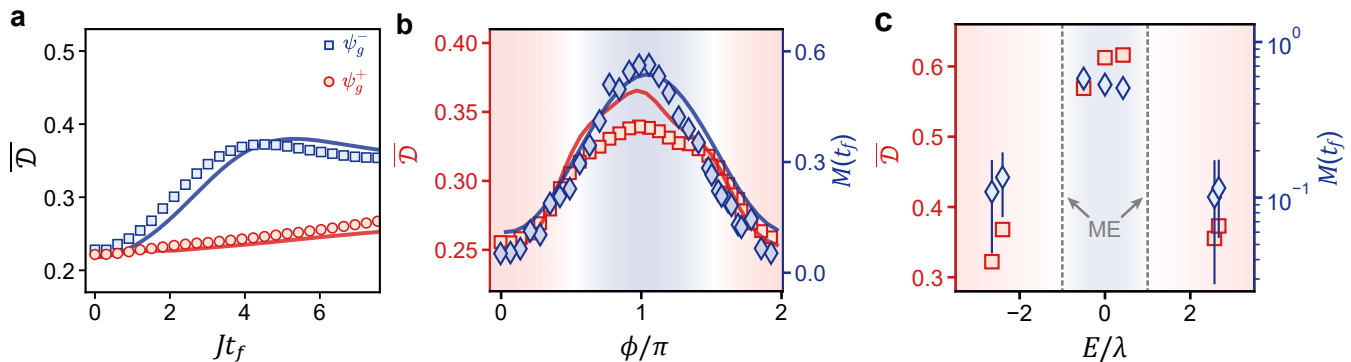


FIG. 4. **Mobility edges in the quasiperiodic mosaic lattice.** **a** Measured time-averaged observable $\overline{\mathcal{D}}$, where the system is quenched from the localized state ψ_g^+ and zero-energy state ψ_g^- of the Hamiltonian H as $\lambda \rightarrow 0$ with $|\psi_g^\pm\rangle = (|1\rangle_{12} \pm |1\rangle_{13})/\sqrt{2}$. The site j ranging from 1 to $N = 24$ and $\theta = \pi/5$. **b-c** Measured $\overline{\mathcal{D}}$ and $M(t_f)$ for the system quenched from the superposition of localized and critical state $\psi_n^0 = (|1\rangle_{12} + e^{i\phi}|1\rangle_{13})/\sqrt{2}$ (**b**), as well as for states ψ_n^\pm located near the edge (inside the novel mobility edges) and center (outside the novel mobility edges) of the spectrum (**c**), where $t_f = 300$ ns and $\psi_n^\pm = (|1\rangle_n \pm |1\rangle_{n+1})/\sqrt{2}$. The dashed lines mark the mobility edges separating the localized and critical states. The markers represent experimental data, and the solid lines correspond to numerical simulations.

during early-time dynamics and serves as a complementary metric. In the following, we conduct our experiment using a total of 24 qubits, as the dynamics near the IDZs do not require the full 56 qubits within the relevant time scale as shown in Fig. 2d-f. For instance, we present the time-averaged observable $\overline{\mathcal{D}}$ within the time range from 0 to t_f for typical critical (localized) phases as $\lambda/J = 2$ ($\lambda/J = 1/4$) in Fig. 3a, by initializing the system in the state $|\psi(t=0)\rangle = |1\rangle_{14}$ located near the IDZ, which exhibits the most distinct behaviors in Fig. 2. We then benchmark the phase diagram of the mosaic model in Fig. 3b. By varying λ/J from 0 to 2.5 while maintaining $J/(2\pi) = 4$ MHz and $t_f = 300$ ns, the system transitions from a deeply localized phase to a critical phase. This transition is evidenced by the increase of $\overline{\mathcal{D}}$ from nearly zero to a saturate plateau about 0.4, and the corresponding increase of $M(t_f)$ from vanishingly small to a finite value. The nearly simultaneous saturation of $\overline{\mathcal{D}}$ and $M(t_f)$ signals a phase transition between localized ($\lambda < J$) and critical phase ($\lambda > J$) near $\lambda/J = 1$, matching well the theoretical calculations.

With the long-range couplings, we experimentally uncover a generalized mechanism that IDZs and critical states are robust to weak $J_{m,n}^L$. The transition from critical to extended states occurs only when $J_{m,n}^L$ exceeds a threshold, and can be observed by measuring the characteristic uni-side propagation dynamics of critical states. We quantify the observation through the time-averaged density population across IDZ (say at $j = j_0$) observed in above section $\overline{n}_r = \sum_{j > j_0} n_j$. The critical state turns to an extended one when both \overline{n}_r and $\overline{\mathcal{D}}$ saturate, indicating the breakdown of uni-side dynamics and the IDZs' fully disappearing. As shown in Fig. 3c, the small long-range coupling does not ruin the critical states, with $\overline{n}_r \approx 0$. Instead, the IDZs of the dominating J_i -terms are dressed by long-range couplings, and stabilize the criti-

cal states in this regime. When the long-range coupling exceeds a threshold $J_{m,n}^L/J \gtrsim 0.4$, both $\overline{\mathcal{D}}$ and \overline{n}_r saturate as marked by the blue shadow, consistent with the numerical results. In theory, we model the dressed IDZs due to the next-nearest-neighbor couplings, and show the critical-extended phase transition analytically by renormalization group method, consistent with the experimental observation (see Supplementary Material).

To further illustrate the transition between critical and extended phases, we also measure the phase diagram versus λ with fixed long-range coupling $J_{m,n}^L$, as shown in Fig. 3d. Turning on a large uniform long-range coupling $J_{m,n}^L = 2.5J$ always drives the system at any λ into an extended phase, while increasing λ further delocalizes the system, resulting in larger accumulated $\overline{\mathcal{D}}$ and wider $M(t_f)$ compared to the case $\lambda = 0$. This feature further confirms the transition from critical to extended phase under large $J_{m,n}$. These measurements show the rigorous criteria for quantum critical states: the IDZs in the dominating hopping couplings J_j and the delocalized nature in the regime $\lambda > J$. The two criteria guarantee the self-similar and scale-invariance of critical states.

Probing mobility edges. Having established the experimental detection and characterization of critical states, we can probe the new MEs between critical and localized states¹¹. For this we turn off long-range couplings but switch on the quasiperiodic potential V_j . From numerical results, we show when V_0/J is small, only the edges of the spectrum remain localized, while for $V_0 \gg J$, most of the spectrum becomes localized (see Supplementary Material). At the high symmetry line $V_0 = J$, the system is again exactly solvable, yielding MEs at $E_c = \pm\lambda$, with critical (localized) states for the region $|E| < |\lambda|$ ($|E| > |\lambda|$). In particular, in this regime the ratio of localized to critical states is 1 : 1, which facilitates the probe of MEs between the two types of states.

We measure the MEs for $V_0/J = 1$ by setting $J/(2\pi) =$

4 MHz in the experiment. We start by demonstrating the ME enriched quench dynamics of entangled states near the IDZ. Specifically, we initialize the system in $|\psi_g^\pm\rangle = (|1\rangle_{12} \pm |1\rangle_{13})/\sqrt{2}$, which are eigenstates of the Hamiltonian for $\lambda \rightarrow 0$. We then evolve the initial states under the Hamiltonian at $\lambda/J = 1/4$. In Fig. 4a, \overline{D} of the initially localized state ψ_g^+ (ψ_g^-) displays a slow (fast) accumulation. Such qualitatively different dynamics of $|\psi_g^\pm\rangle$ within the same parameter of the system, indicating the presence of ME in the system. We further incorporate more initial states with energies by adjusting the relative phase ϕ of the state $\psi_g^\phi = (|1\rangle_{12} + e^{i\phi}|1\rangle_{13})/\sqrt{2}$. As shown in Fig. 4b, $M(t_f)$ displays a non-trivial pattern of rise-fall as the ϕ evolves, and \overline{D} shows a similar trend. This indicates that the changes in ϕ alter the ratio of localized to critical states, leading to distinct dynamics and suggesting the coexistence of these states within the spectrum resulted by the MEs.

Finally, we probe the localized-to-critical transition behavior as the initial energies cross the ME: $|E| = \lambda$ with $\lambda/J = 1.5$ and the initial states $\psi_n^\pm = (|1\rangle_n \pm |1\rangle_{n+1})/\sqrt{2}$ for various n , as shown in Fig. 4c. Here, the initial states $\psi_n^\pm = (|1\rangle_n \pm |1\rangle_{n+1})/\sqrt{2}$ are chosen to realize typical energies both inside and outside the MEs, with $n = \{4, 8, 10, 12, 16, 18\}$ for the plus sign and an additional $n = 18$ for the minus sign. When the initial states are prepared as $|E| > \lambda$, the \overline{D} and $M(t_f)$ saturates a small number, corresponding to large amount of localized orbitals of such initial states. Conversely, if the initial state is prepared near the center of the spectrum ($|E| < \lambda$), its dynamics displays clear critical characteristics with much larger $M(t_f)$ accompanied with $\overline{D} \sim 0.62$. This highlights that $E_c = \pm\lambda$ serves as a critical threshold for the energy-dependent spin dynamics spreading, effectively separating the localized and critical orbitals.

Discussion and outlook.

In this work, we experimentally confirm the presence of quantum critical states in a superconducting quantum simulator with tunable (long-range) couplings and on-site potentials. We unveil a generalized mechanism of critical states, highlighting the role of incommensu-

rately distributed zeros (IDZs) in stabilizing the critical state. Our study also explores the localized-to-critical transition, and critical-to-extended transition, showing that critical states persist as long as quasiperiodic zeros are not disrupted by long-range couplings. We further investigate the mobility edges between critical and localized states, revealing enriched spin evolution and energy-dependent quench dynamics near the IDZs.

This study established a standard to rigorously characterize the critical states in experiment, applicable to broad range of quantum simulation and quantum computing systems, and provided a versatile platform to further explore novel quantum physics of critical states, in particular for higher dimensional systems and the many-body regime. For instance, the inter-particle interactions can be introduced by incorporating anharmonicity in the qubits⁷³, and shall lead to the emergence of novel phases that have not been precisely observed before. The multifractal nature of critical states renders the ground phase of the system highly sensitive to interactions, enriching the exotic symmetry-breaking phases^{18,24–28}. For higher energy states, the non-interacting critical states turn to many-body critical phases²⁹—a third type of fundamental phase in disordered system, which is different from the thermal phase and many-body localization. Building on the present setting, these highly important quantum many-body phases hold the promise for our next studies.

Beyond the closed system framework, the 2D array of tunably coupled qubits offers high controllability of noise^{74,75}, enabling the in-depth study of the robustness of critical states and anomalous MEs against decoherence. Also, by combining our tunable qubits with tailored dissipation, one can explore dissipation-induced critical phases and mobility edges^{76,77}. Moreover, the combination of many-body interactions and controlled noise opens up the way to experimentally probe transitions between many-body critical phase in open systems and generic thermalized states. This is an area that remains unexplored both theoretically and experimentally, yet is of fundamental importance.

-
- [1] P. W. Anderson, *Absence of diffusion in certain random lattices*, *Phys. Rev.* **109**, 1492 (1958).
 - [2] E. Abrahams, P. W. Anderson, D. C. Licciardello, and T. V. Ramakrishnan, *Scaling theory of localization: Absence of quantum diffusion in two dimensions*, *Phys. Rev. Lett.* **42**, 673 (1979).
 - [3] P. A. Lee and T. V. Ramakrishnan, *Disordered electronic systems*, *Rev. Mod. Phys.* **57**, 287 (1985).
 - [4] B. Kramer and A. MacKinnon, *Localization: Theory and experiment*, *Rep. Prog. Phys.* **56**, 1469 (1993).
 - [5] F. Evers and A. D. Mirlin, *Anderson transitions*, *Rev. Mod. Phys.* **80**, 1355 (2008).
 - [6] Y. Hatsugai and M. Kohmoto, *Energy spectrum and the quantum Hall effect on the square lattice with next-nearest-neighbor hopping*, *Phys. Rev. B* **42**, 8282 (1990).
 - [7] J. H. Han, D. J. Thouless, H. Hiramoto, and M. Kohmoto, *Critical and bicritical properties of Harper's equation with next-nearest-neighbor coupling*, *Phys. Rev. B* **50**, 11365 (1994).
 - [8] J. Wang, X.-J. Liu, G. Xianlong, and H. Hu, *Phase diagram of a non-Abelian Aubry-André-Harper model with p-wave superfluidity*, *Phys. Rev. B* **93**, 104504 (2016).
 - [9] Y. Wang, C. Cheng, X.-J. Liu, and D. Yu, *Many-Body Critical Phase: Extended and Nonthermal*, *Phys. Rev. Lett.* **126**, 080602 (2021).
 - [10] Y. Wang, L. Zhang, W. Sun, T.-F. J. Poon, and X.-J. Liu, *Quantum phase with coexisting localized, extended, and critical zones*, *Phys. Rev. B* **106**, L142023 (2022).

- [11] X.-C. Zhou, Y. Wang, T.-F. J. Poon, Q. Zhou, and X.-J. Liu, *Exact new mobility edges between critical and localized states*, *Phys. Rev. Lett.* **131**, 176401 (2023).
- [12] F. A. An, E. J. Meier, and B. Gadway, *Engineering a Flux-Dependent Mobility Edge in Disordered Zigzag Chains*, *Phys. Rev. X* **8**, 031045 (2018).
- [13] H. P. Lüschen, S. Scherg, T. Kohlert, M. Schreiber, P. Bordia, X. Li, S. Das Sarma, and I. Bloch, *Single-Particle Mobility Edge in a One-Dimensional Quasiperiodic Optical Lattice*, *Phys. Rev. Lett.* **120**, 160404 (2018).
- [14] T. Kohlert, S. Scherg, X. Li, H. P. Lüschen, S. Das Sarma, I. Bloch, and M. Aidelsburger, *Observation of Many-Body Localization in a One-Dimensional System with a Single-Particle Mobility Edge*, *Phys. Rev. Lett.* **122**, 170403 (2019).
- [15] F. A. An, K. Padavić, E. J. Meier, S. Hegde, S. Ganeshan, J. H. Pixley, S. Vishveshwara, and B. Gadway, *Interactions and Mobility Edges: Observing the Generalized Aubry-André Model*, *Phys. Rev. Lett.* **126**, 040603 (2021).
- [16] Y. Wang, J.-H. Zhang, Y. Li, J. Wu, W. Liu, F. Mei, Y. Hu, L. Xiao, J. Ma, C. Chin, and S. Jia, *Observation of interaction-induced mobility edge in an atomic Aubry-André wire*, *Phys. Rev. Lett.* **129**, 103401 (2022).
- [17] J. Gao, I. M. Khaymovich, X.-W. Wang, Z.-S. Xu, A. Iovan, G. Krishna, J. Jiens, A. Cataldo, A. V. Balatsky, V. Zwiller, and A. W. Elshaari, *Probing multi-mobility edges in quasiperiodic mosaic lattices*, *Sci. Bull.* **70**, 58 (2025).
- [18] X.-J. Liu, *Quantum matter in multifractal patterns*, *Nat. Phys.* **20**, 1851 (2024).
- [19] T. C. Halsey, M. H. Jensen, L. P. Kadanoff, I. Procaccia, and B. I. Shraiman, *Fractal measures and their singularities: The characterization of strange sets*, *Phys. Rev. A* **33**, 1141 (1986).
- [20] R. Ketzmerick, K. Kruse, S. Kraut, and T. Geisel, *What determines the spreading of a wave packet?*, *Phys. Rev. Lett.* **79**, 1959 (1997).
- [21] A. D. Mirlin, Y. V. Fyodorov, A. Mildenerger, and F. Evers, *Exact relations between multifractal exponents at the anderson transition*, *Phys. Rev. Lett.* **97**, 046803 (2006).
- [22] R. Dubertrand, I. García-Mata, B. Georgeot, O. Giraud, G. Lemarié, and J. Martin, *Two scenarios for quantum multifractality breakdown*, *Phys. Rev. Lett.* **112**, 234101 (2014).
- [23] H. Yao, A. Khoudli, L. Bresque, and L. Sanchez-Palencia, *Critical behavior and fractality in shallow one-dimensional quasiperiodic potentials*, *Phys. Rev. Lett.* **123**, 070405 (2019).
- [24] M. V. Feigel'man, L. B. Ioffe, V. E. Kravtsov, and E. A. Yuzbashyan, *Eigenfunction Fractality and Pseudogap State near the Superconductor-Insulator Transition*, *Phys. Rev. Lett.* **98**, 027001 (2007).
- [25] I. S. Burmistrov, I. V. Gornyi, and A. D. Mirlin, *Enhancement of the Critical Temperature of Superconductors by Anderson Localization*, *Phys. Rev. Lett.* **108**, 017002 (2012).
- [26] K. Zhao, H. Lin, X. Xiao, W. Huang, W. Yao, M. Yan, Y. Xing, Q. Zhang, Z.-X. Li, S. Hoshino, J. Wang, S. Zhou, L. Gu, M. S. Bahramy, H. Yao, N. Nagaosa, Q.-K. Xue, K. T. Law, X. Chen, and S.-H. Ji, *Disorder-induced multifractal superconductivity in monolayer niobium dichalcogenides*, *Nat. Phys.* **15**, 904 (2019).
- [27] B. Sacépé, M. Feigel'man, and T. M. Klapwijk, *Quantum breakdown of superconductivity in low-dimensional materials*, *Nat. Phys.* **16**, 734 (2020).
- [28] M. Gonçalves, B. Amorim, F. Riche, E. V. Castro, and P. Ribeiro, *Incommensurability enabled quasi-fractal order in 1D narrow-band moiré systems*, *Nat. Phys.* **20**, 1933 (2024).
- [29] Y. Wang, L. Zhang, S. Niu, D. Yu, and X.-J. Liu, *Realization and Detection of Nonergodic Critical Phases in an Optical Raman Lattice*, *Phys. Rev. Lett.* **125**, 073204 (2020).
- [30] A. P. Luca D'Alessio, Yariv Kafri and M. Rigol, *From quantum chaos and eigenstate thermalization to statistical mechanics and thermodynamics*, *Adv. Phys.* **65**, 239 (2016).
- [31] J. M. Deutsch, *Quantum statistical mechanics in a closed system*, *Phys. Rev. A* **43**, 2046 (1991).
- [32] M. Rigol, V. Dunjko, and M. Olshanii, *Thermalization and its mechanism for generic isolated quantum systems*, *Nature* **452**, 854 (2008).
- [33] M. Srednicki, *Chaos and quantum thermalization*, *Phys. Rev. E* **50**, 888 (1994).
- [34] A. Avila, *Global theory of one-frequency Schrödinger operators*, *Acta Mathematica* **215**, 1 (2015).
- [35] M. Rispoli, A. Lukin, R. Schittko, S. Kim, M. E. Tai, J. Léonard, and M. Greiner, *Quantum critical behaviour at the many-body localization transition*, *Nature* **573**, 385 (2019).
- [36] V. Goblot, A. Štrkalj, N. Pernet, J. L. Lado, C. Dorow, A. Lemaître, L. Le Gratiet, A. Harouri, I. Sagnes, S. Ravets, A. Amo, J. Bloch, and O. Zilberberg, *Emergence of criticality through a cascade of delocalization transitions in quasiperiodic chains*, *Nat. Phys.* **16**, 832 (2020).
- [37] T. Xiao, D. Xie, Z. Dong, T. Chen, W. Yi, and B. Yan, *Observation of topological phase with critical localization in a quasi-periodic lattice*, *Sci. Bull.* **66**, 2175 (2021).
- [38] H. Li, Y.-Y. Wang, Y.-H. Shi, K. Huang, X. Song, G.-H. Liang, Z.-Y. Mei, B. Zhou, H. Zhang, J.-C. Zhang, S. Chen, S. P. Zhao, Y. Tian, Z.-Y. Yang, Z. Xiang, K. Xu, D. Zheng, and H. Fan, *Observation of critical phase transition in a generalized Aubry-André-Harper model with superconducting circuits*, *npj Quantum Inf.* **9**, 40 (2023).
- [39] T. Shimasaki, M. Prichard, H. E. Kondakci, J. E. Pagett, Y. Bai, P. Dotti, A. Cao, A. R. Dardia, T.-C. Lu, T. Grover, and D. M. Weld, *Anomalous localization in a kicked quasicrystal*, *Nat. Phys.* **20**, 409 (2024).
- [40] J.-B. Suck, M. Schreiber, P. Häussler, R. Hull, R. M. Osgood, J. Parisi, and A. Zunger, eds., *Quasicrystals: An Introduction to Structure, Physical Properties and Applications*, Springer Series in Materials Science, Vol. 55 (Springer Berlin Heidelberg, Berlin, Heidelberg, 2002).
- [41] S. Aubry and G. André, *Analyticity breaking and anderson localization in incommensurate lattices*, *Ann. Israel Phys. Soc.* **3**, 18 (1980).
- [42] G. Roati, C. D'Errico, L. Fallani, M. Fattori, C. Fort, M. Zaccanti, G. Modugno, M. Modugno, and M. Inguscio, *Anderson localization of a non-interacting Bose-Einstein condensate*, *Nature* **453**, 895 (2008).
- [43] J. Biddle and S. Das Sarma, *Predicted Mobility Edges in One-Dimensional Incommensurate Optical Lattices: An Exactly Solvable Model of Anderson Localization*, *Phys. Rev. Lett.* **104**, 070601 (2010).

- [44] S. Ganeshan, J. H. Pixley, and S. Das Sarma, *Nearest Neighbor Tight Binding Models with an Exact Mobility Edge in One Dimension*, *Phys. Rev. Lett.* **114**, 146601 (2015).
- [45] X. Deng, S. Ray, S. Sinha, G. V. Shlyapnikov, and L. Santos, *One-Dimensional Quasicrystals with Power-Law Hopping*, *Phys. Rev. Lett.* **123**, 025301 (2019).
- [46] H. Yao, A. Khoufli, L. Bresque, and L. Sanchez-Palencia, *Critical Behavior and Fractality in Shallow One-Dimensional Quasiperiodic Potentials*, *Phys. Rev. Lett.* **123**, 070405 (2019).
- [47] Y. Wang, X. Xia, L. Zhang, H. Yao, S. Chen, J. You, Q. Zhou, and X.-J. Liu, *One-Dimensional Quasiperiodic Mosaic Lattice with Exact Mobility Edges*, *Phys. Rev. Lett.* **125**, 196604 (2020).
- [48] S. Longhi, *Resonances, mobility edges, and gap-protected Anderson localization in generalized disordered mosaic lattices*, *Phys. Rev. B* **110**, 184201 (2024).
- [49] C. Neill, T. McCourt, X. Mi, Z. Jiang, M. Y. Niu, W. Mruzckiewicz, I. Aleiner, F. Arute, K. Arya, J. Atalaya, *et al.*, *Accurately computing the electronic properties of a quantum ring*, *Nature* **594**, 508 (2021).
- [50] X. Mi, M. Ippoliti, C. Quintana, A. Greene, Z. Chen, J. Gross, F. Arute, K. Arya, J. Atalaya, R. Babbush, *et al.*, *Time-crystalline eigenstate order on a quantum processor*, *Nature* **601**, 531 (2021).
- [51] K. Satzinger, Y.-J. Liu, A. Smith, C. Knapp, M. Newman, C. Jones, Z. Chen, C. Quintana, X. Mi, A. Dunsworth, *et al.*, *Realizing topologically ordered states on a quantum processor*, *Science* **374**, 1237 (2021).
- [52] X. Mi, P. Roushan, C. Quintana, S. Mandrà, J. Marshall, C. Neill, F. Arute, K. Arya, J. Atalaya, R. Babbush, *et al.*, *Information scrambling in quantum circuits*, *Science* **374**, 1479 (2021).
- [53] X. Mi, M. Sonner, M. Y. Niu, K. W. Lee, B. Foxen, R. Acharya, I. Aleiner, T. I. Andersen, F. Arute, K. Arya, *et al.*, *Noise-resilient edge modes on a chain of superconducting qubits*, *Science* **378**, 785 (2022).
- [54] A. Morvan, T. I. Andersen, X. Mi, C. Neill, A. Petukhov, K. Kechedzhi, D. A. Abanin, A. Michailidis, R. Acharya, F. Arute, *et al.*, *Formation of robust bound states of interacting microwave photons*, *Nature* **612**, 240 (2022).
- [55] B. Saxberg, A. Vrajitoarea, G. Roberts, M. G. Panetta, J. Simon, and D. I. Schuster, *Disorder-assisted assembly of strongly correlated fluids of light*, *Nature* **612**, 435 (2022).
- [56] A. H. Karamlou, I. T. Rosen, S. E. Muschinske, C. N. Barrett, A. D. Paolo, L. Ding, P. M. Harrington, M. Hays, R. Das, D. K. Kim, B. M. Niedzielski, M. Schuldt, K. Serniak, M. E. Schwartz, J. L. Yoder, S. Gustavsson, Y. Yanay, J. A. Grover, and W. D. Oliver, *Probing entanglement in a 2d hard-core bose-hubbard lattice*, *Nature* **629**, 561 (2024).
- [57] J. Braumüller, A. H. Karamlou, Y. Yanay, B. Kannan, D. Kim, M. Kjaergaard, A. Melville, B. M. Niedzielski, Y. Sung, A. Vepsäläinen, R. Winik, J. L. Yoder, T. P. Orlando, S. Gustavsson, C. Tahan, and W. D. Oliver, *Probing quantum information propagation with out-of-time-ordered correlators*, *Nat. Phys.* **18**, 172 (2021).
- [58] A. H. Karamlou, J. Braumüller, Y. Yanay, A. Di Paolo, P. M. Harrington, B. Kannan, D. Kim, M. Kjaergaard, A. Melville, S. Muschinske, B. M. Niedzielski, A. Vepsäläinen, R. Winik, J. L. Yoder, M. Schwartz, C. Tahan, T. P. Orlando, S. Gustavsson, and W. D. Oliver, *Quantum transport and localization in 1d and 2d tight-binding lattices*, *npj Quantum Inf.* **8**, 35 (2022).
- [59] I. T. Rosen, S. Muschinske, C. N. Barrett, D. A. Rower, R. Das, D. K. Kim, B. M. Niedzielski, M. Schuldt, K. Serniak, M. E. Schwartz, J. L. Yoder, J. A. Grover, and W. D. Oliver, *Flat-band (de)localization emulated with a superconducting qubit array*, *arXiv preprint, arXiv:2410.07878* (2024).
- [60] I. T. Rosen, S. Muschinske, C. N. Barrett, A. Chatterjee, M. Hays, M. A. DeMarco, A. H. Karamlou, D. A. Rower, R. Das, D. K. Kim, B. M. Niedzielski, M. Schuldt, K. Serniak, M. E. Schwartz, J. L. Yoder, J. A. Grover, and W. D. Oliver, *A synthetic magnetic vector potential in a 2d superconducting qubit array*, *Nat. Phys.* **20**, 1881 (2024).
- [61] R. Ma, B. Saxberg, C. Owens, N. Leung, Y. Lu, J. Simon, and D. I. Schuster, *A dissipatively stabilized Mott insulator of photons*, *Nature* **566**, 51 (2019).
- [62] B. Du, R. Suresh, S. López, J. Cadiente, and R. Ma, *Probing site-resolved current in strongly interacting superconducting circuit lattices*, *Phys. Rev. Lett.* **133**, 060601 (2024).
- [63] B. Du, Q. Guo, S. López, and R. Ma, *Tunneling spectroscopy in superconducting circuit lattices*, *arXiv preprint, arXiv:2411.07997* (2024).
- [64] M. Gong, S. Wang, C. Zha, M.-C. Chen, H.-L. Huang, Y. Wu, Q. Zhu, Y. Zhao, S. Li, S. Guo, *et al.*, *Quantum walks on a programmable two-dimensional 62-qubit superconducting processor*, *Science* **372**, 948 (2021).
- [65] F. Chen, Z.-H. Sun, M. Gong, Q. Zhu, Y.-R. Zhang, Y. Wu, Y. Ye, C. Zha, S. Li, S. Guo, H. Qian, H.-L. Huang, J. Yu, H. Deng, H. Rong, J. Lin, Y. Xu, L. Sun, C. Guo, N. Li, F. Liang, C.-Z. Peng, H. Fan, X. Zhu, and J.-W. Pan, *Observation of strong and weak thermalization in a superconducting quantum processor*, *Phys. Rev. Lett.* **127**, 020602 (2021).
- [66] Z.-C. Xiang, K. Huang, Y.-R. Zhang, T. Liu, Y.-H. Shi, C.-L. Deng, T. Liu, H. Li, G.-H. Liang, Z.-Y. Mei, H. Yu, G. Xue, Y. Tian, X. Song, Z.-B. Liu, K. Xu, D. Zheng, F. Nori, and H. Fan, *Simulating chern insulators on a superconducting quantum processor*, *Nat. Commun.* **14**, 5433 (2023).
- [67] Y.-H. Shi, Y. Liu, Y.-R. Zhang, Z. Xiang, K. Huang, T. Liu, Y.-Y. Wang, J.-C. Zhang, C.-L. Deng, G.-H. Liang, Z.-Y. Mei, H. Li, T.-M. Li, W.-G. Ma, H.-T. Liu, C.-T. Chen, T. Liu, Y. Tian, X. Song, S. P. Zhao, K. Xu, D. Zheng, F. Nori, and H. Fan, *Quantum simulation of topological zero modes on a 41-qubit superconducting processor*, *Phys. Rev. Lett.* **131**, 080401 (2023).
- [68] Y.-H. Shi, Z.-H. Sun, Y.-Y. Wang, Z.-A. Wang, Y.-R. Zhang, W.-G. Ma, H.-T. Liu, K. Zhao, J.-C. Song, G.-H. Liang, Z.-Y. Mei, J.-C. Zhang, H. Li, C.-T. Chen, X. Song, J. Wang, G. Xue, H. Yu, K. Huang, Z. Xiang, K. Xu, D. Zheng, and H. Fan, *Probing spin hydrodynamics on a superconducting quantum simulator*, *Nat. Commun.* **15**, 7573 (2024).
- [69] Y. Yao, L. Xiang, Z. Guo, Z. Bao, Y.-F. Yang, Z. Song, H. Shi, X. Zhu, F. Jin, J. Chen, *et al.*, *Observation of many-body fock space dynamics in two dimensions*, *Nat. Phys.* **19**, 1459 (2023).
- [70] P. Zhang, H. Dong, Y. Gao, L. Zhao, J. Hao, J.-Y. Desaulles, Q. Guo, J. Chen, J. Deng, B. Liu, W. Ren, Y. Yao, X. Zhang, S. Xu, K. Wang, F. Jin, X. Zhu, B. Zhang, H. Li, C. Song, Z. Wang, F. Liu, Z. Papić, L. Ying,

- H. Wang, and Y.-C. Lai, *Many-body hilbert space scarring on a superconducting processor*, *Nat. Phys.* **19**, 120 (2022).
- [71] X. Zhang, W. Jiang, J. Deng, K. Wang, J. Chen, P. Zhang, W. Ren, H. Dong, S. Xu, Y. Gao, F. Jin, X. Zhu, Q. Guo, H. Li, C. Song, A. V. Gorshkov, T. Iadecola, F. Liu, Z.-X. Gong, Z. Wang, D.-L. Deng, and H. Wang, *Digital quantum simulation of floquet symmetry-protected topological phases*, *Nature* **607**, 468 (2022).
- [72] Y. Xu, J. Chu, J. Yuan, J. Qiu, Y. Zhou, L. Zhang, X. Tan, Y. Yu, S. Liu, J. Li, *et al.*, *High-fidelity, high-scalability two-qubit gate scheme for superconducting qubits*, *Phys. Rev. Lett.* **125**, 240503 (2020).
- [73] Z. Tao, W. Huang, J. Niu, L. Zhang, Y. Ke, X. Gu, L. Lin, J. Qiu, X. Sun, X. Yang, J. Zhang, J. Zhang, Y. Zhou, X. Deng, C. Hu, L. Hu, J. Li, Y. Liu, D. Tan, Y. Xu, T. Yan, Y. Chen, C. Lee, Y. Zhong, S. Liu, and D. Yu, *Emulating Thouless pumping in the interacting Rice-Mele model using superconducting qubits*, *Front. Phys.* **20**, 033202.
- [74] Z. Tao, F. Schmolke, C.-K. Hu, W. Huang, Y. Zhou, J. Zhang, J. Chu, L. Zhang, X. Sun, Z. Guo, J. Niu, W. Weng, S. Liu, Y. Zhong, D. Tan, D. Yu, and E. Lutz, *Noise-induced quantum synchronization and maximally entangled mixed states in superconducting circuits*, *arXiv preprint*, [arXiv:2406.10457](https://arxiv.org/abs/2406.10457) (2024).
- [75] Y. Liang, C. Xie, Z. Guo, P. Huang, W. Huang, Y. Liu, J. Qiu, X. Sun, Z. Wang, X. Yang, *et al.*, *Dephasing-assisted diffusive dynamics in superconducting quantum circuits*, *arXiv preprint*, [arXiv:2411.15571](https://arxiv.org/abs/2411.15571) (2024).
- [76] S. Longhi, *Dephasing-Induced Mobility Edges in Quasicrystals*, *Phys. Rev. Lett.* **132**, 236301 (2024).
- [77] Y. Liu, Z. Wang, C. Yang, J. Jie, and Y. Wang, *Dissipation-Induced Extended-Localized Transition*, *Phys. Rev. Lett.* **132**, 216301 (2024).

Data availability

The data that support the plots within this paper and other findings of this study are available from the corresponding authors upon request.

Code availability

All the relevant source codes are available from the corresponding authors upon request.

Acknowledgements This work was supported by the Innovation Program for Quantum Science and Technology (Grant No. 2021ZD0301703 and No.2021ZD0302000), the Science, Technology and Innovation Commission of Shenzhen Municipality (KQTD20210811090049034), National Key Research and Development Program of China (2021YFA1400900), the National Natural Science Foundation of China (Grants No.12174178, No.12425401 and No.12261160368).

Author contributions

W.H. designed and tested the device. Libo Z. and Yuxuan Z. fabricated the device under the supervision of S.L. Z.T. collected and analyzed the data. X.-C.Z. provided theoretical and numerical studies under the supervision of X.-J.L. Jiawei Z. built the microwave electronics. Youpeng Z., X.-J.L. and D.Y. supervised the project. All authors contributed to the discussion and preparation of the manuscript.

Competing interests

The authors declare no competing interests.